Source Directivity Simulation in Digital Waveguide Mesh-based Room Acoustics Models

Hüseyin Hacıhabiboğlu, Banu Günel, and Ahmet M. Kondoz

Multimedia and DSP Research Group (I-Lab), Centre for Communication Systems Research (CCSR), University of Surrey, Guildford, Surrey, GU2 7XH, United Kingdom

Correspondence should be addressed to Hüseyin Hacıhabiboğlu (h.hacihabiboglu@surrey.ac.uk)

ABSTRACT

Digital waveguide meshes provide a computationally simple physical modelling approach for simulating wave propagation inside enclosures such as rooms. A digital waveguide mesh allows access both to the pressure values at scattering junctions and to the incoming and outgoing wave variables at those junctions. It is thus possible to access both the pressure and the velocity components of the simulated sound field. This paper proposes a simple method to excite a digital waveguide mesh with outgoing wave variables at the scattering junctions to simulate sound propagation from directional sources. Two examples are given for the 2D digital waveguide mesh to demonstrate the utility of the method.

1. INTRODUCTION

Acoustical models of rooms have important uses not only for testing the feasibility or usefulness of acoustical designs for architectural considerations, but also for the purpose of realistic auralisation in virtual and augmented reality systems, and advanced telecommunication applications [1]. There are three main groups of such models: wave-based models, geometrical models, and statistical models. The first two groups are widely used in practical auralisation applications [2].

Wave-based methods provide numerical solutions of the wave equation. The room response at any given position can be obtained up to the level of approximation provided by the respective model. Among these numerical solvers, finite and boundary element methods (FEM and BEM) operate in the frequency domain. Similarly, finite difference time domain (FDTD), digital waveguide models (DWG) and other similar models provide temporal solutions of the wave equation. The advantage of these methods is that, they provide a discrete time and discrete space solution of the wave equation. Therefore, simulation of wave related phenomena (such as diffraction, occlusion etc.) requires no additional computational effort.

All real sound sources (e.g. human mouth [3, 4], musical instruments [5] etc.) radiate sound unevenly towards different directions and for different frequencies. It is therefore essential to include the source directivity in the acoustical model in order to simulate real sound sources better. With geometrical methods such as the image-source method [6], special directional filters are designed for a finite number of sampled solid angles and the direct sound and the early reflections are filtered with those to obtain an approximation to source directivity [7], or as with ray tracing [8] the distribution of rays emitted may be selected accordingly.

Two methods to simulate directive sources in DWG meshes are proposed in this paper: (1) When an analytic source directivity function exists for the source the directive velocity potential concept is used to obtain a velocity field with which the DWG mesh is initialised, and (2) when an empirical directivity function of a source is avaliable, with which the intermediate velocity field is directively weighted.

This paper is organised as follows. Section 2 provides a brief summary of digital waveguide mesh models. Section 3 reviews source directivity, shows the relation between different acoustical parameters for a directive source, and presents the method proposed with room acoustics simulations based on DWG mesh models. Section 4 presents simulation results for two different directive sources using the proposed method.

2. DIGITAL WAVEGUIDE MESH MODELLING

Digital waveguides (DWG) are a family of very simple, first-order finite-difference solvers for the wave equation in the time domain. DWGs have successfully been used in a number of acoustical modelling problems such as the modelling of the vocal tract [9], vibrating strings [10, 11], drum membranes [12], and room acoustics [13]

2.1. Junction equations

A digital waveguide mesh is composed of scattering junctions (i.e. nodes), bidirectional delays, and boundary elements. Each scattering junction ($S_{x,y}$) is connected to a number of other junctions with the bidirectional delays over their input and output ports. Pressure values at each port ($p_{J,i}$) and the junction pressure (p_J) are equal to each other, and the sum of all port particle velocities ($v_{J,i}$) of the given junction is zero. For an N-port junction this amounts to:

$$p_{J,1} = p_{J,2} = \cdots = p_{J,N} = p_J, \tag{1}$$

$$\sum_{i=1}^{N} v_{J,i} = 0 \tag{2}$$

The flow variables (i.e. corresponding to *fluid velocity*) at port i, $vc_{J,i}$ is defined as:

$$v_{J,i} = Y_i \left(p^-_{J,i} - p^+_{J,i} \right) \tag{3}$$

where $p^+_{J,i}$ and $p^-_{J,i}$ are the incident and reflected pressure wave variables at the port i respectively, and Y_i is the port admittance [14].

2.2. 2D Rectilinear DWG

Although a 3D model is necessary for simulating wave propagation inside enclosures, it has been shown that a 2D model can also be used to demonstrate basic wave propagation on a particular plane [15, 16]. There are only three regular discretisation strategies for a plane. These are triangular, hexagonal, and rectilinear sampling. All of these discretisation strategies cause direction-dependent dispersion, rectilinear sampling being the less accurate option [17]. However, rectilinear sampling has a particular advantage in the sense that the junctions are more intuitively positioned for post-processing, and that the computational complexity is lower as it requires no multiplications. Further, the direction-dependent dispersion that is the major undesirable consequence of using rectilinear meshes may be mitigated by the use of interpolated DWG meshes [18].

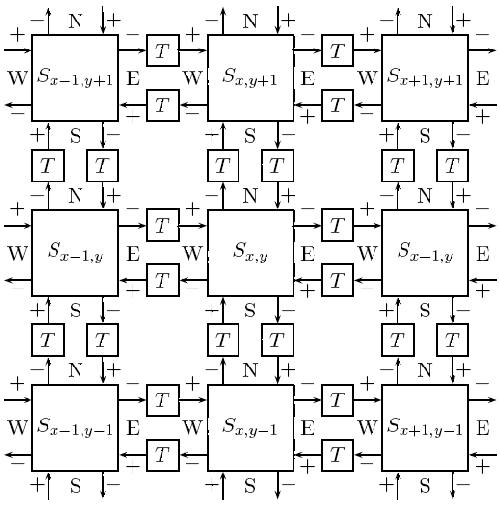

Fig. 1: 2D digital waveguide mesh structure. $S_{x,y}$ are the scattering functions, where T represents a unidirectional delay element.

In a rectilinearly sampled 2D mesh, each node has four ports. A given port can be named geographically as N, S, E, or W depending on its relative orientation in the mesh (see Fig. 1). A two-step iteration scheme is used for obtaining the junction pressures at a given sample time, n. The junction pressure, and outgoing wave variables are calculated as:

$$p_{J,x,y}(n) = \frac{1}{2}\left[p^+_{N,x,y}(n) + p^+_{S,x,y}(n) + p^+_{E,x,y}(n) + p^+_{W,x,y}(n)\right] \tag{4}$$

$$p^-_{N,x,y}(n) = p_{J,x,y}(n) - p^+_{N,x,y}(n), \tag{5}$$

$$p^-_{S,x,y}(n) = p_{J,x,y}(n) - p^+_{S,x,y}(n), \tag{6}$$

$$p^-_{E,x,y}(n) = p_{J,x,y}(n) - p^+_{E,x,y}(n), \tag{7}$$

$$p^-_{W,x,y}(n) = p_{J,x,y}(n) - p^+_{W,x,y}(n), \tag{8}$$

The incident wave variables of neighbouring junctions of a given junction are simply delayed versions of the outgoing wave variables of that junction:

$$p^+_{N,x,y-1}(n+T) = p^-_{S,x,y}(n), \tag{9}$$

$$p^+_{S,x,y+1}(n+T) = p^-_{N,x,y}(n), \tag{10}$$

$$p^+_{E,x-1,y}(n+T) = p^-_{W,x,y}(n), \tag{11}$$

$$p^+_{W,x+1,y}(n+T) = p^-_{E,x,y}(n), \tag{12}$$

where the temporal sampling period, T, is the delay element between junctions.

The calculation of the junction pressure requires four additions and a single left shift operation (i.e. multiplication by $\frac{1}{2}$). The rectilinear DWG mesh is computationally cheap. In addition, the junction positions conveniently coincide with discrete Cartesian coordinates making it easier to use simple analyses and post-processing on the obtained data.

In a simple practical implementation, the iteration explained above is carried out in two consecutive stages:

- *Scattering* is the process carried out in Eqs. 4 and 5-8 by calculating the outgoing wave variables by *scattering* the incoming wave variables. It is possible to skip the calculation of the junction pressure in Eq. 4 and use a matrix multiplication instead for obtaining the outgoing wave variables directly from incident wave variables [14].
- *Propagation* is the shifting of outgoing wave variables within the DWG mesh as shown in Eqs. 9-12 to obtain the incident wave variables for the next iteration.

3. MODELLING SOURCE DIRECTIVITY

3.1. Definition of source directivity

The *source directivity*, $\Gamma_s(\theta,\phi)$, is intimately related to the *radiation pattern* of a source, $J(\theta,\phi)$, defined as the acoustic power radiated per unit solid angle [19].

The instantaneous intensity of the sound field in the radial direction is defined as $\mathbf{I} = p\mathbf{v}$, where p is the pressure and $\mathbf{v}$ is the velocity component of the sound field. The average intensity at a distance, r, is defined as:

$$\overline{\mathbf{I}}(r,\theta,\phi) = \frac{J(\theta,\phi)}{r^2}\mathbf{u}_r, \tag{13}$$

$$= \frac{1}{\Delta T}\int_{t_0}^{t_0+\Delta T} \mathbf{I}(r,\theta,\phi,t)\cdot\mathbf{u}_r\,dt. \tag{14}$$

Then, the radiation pattern of the source, $J(\theta,\phi)$, can be expressed as:

$$J(\theta,\phi) = \frac{r^2}{\Delta T}\int_{t_0}^{t_0+\Delta T} p\,\mathbf{v}\cdot\mathbf{u}_r\,dt. \tag{15}$$

Let us consider the velocity potential, Φ, from which the pressure and velocity parameters can be derived, such that:

$$\mathbf{v} = \nabla\Phi, \qquad p = -\rho\frac{\partial\Phi}{\partial t}, \tag{16}$$

where ρ represents the density, and ∇ denotes the gradient operator.

The velocity potential for an omnidirectional spherically symmetric source is $\Phi_o(r,t) = -F(t-c^{-1}r)/\rho r$ where F is an arbitrary function of $(t-c^{-1}r)$. It is possible to express omnidirectional velocity and the pressure components as [19]:

$$\mathbf{v}_o(r,t) = \left[\frac{p_o(r,t)}{c\rho r} + \frac{F(t-c^{-1}r)}{\rho r^2}\right]\mathbf{u}_r, \tag{17}$$

$$p_o(r,t) = \frac{1}{r}\frac{\partial}{\partial t}F(t-c^{-1}r). \tag{18}$$

The second term on the r.h.s. of Eq. 17 is inversely propotional to the square of distance from the source and is negligible in the far-field. The radiation pattern in the far-field for an omnidirectional source can thus be defined as:

$$J_o = \frac{1}{r\rho c\Delta T}\int_{t_0}^{t_0+\Delta T} f^2(t-c^{-1}r)\,dt, \tag{19}$$

where $f(t) = dF(t)/dt$. The omnidirectional radiation pattern, J_o, is constant across θ and ϕ as the source has equal intensity for all directions.

Let us define a directional velocity potential, Φ_d, as the omnidirectional velocity potential, Φ_o, weighted by the directivity function, Γ_s, such that:

$$\Phi_d(r,\theta,\phi,t) = \Gamma_s(\theta,\phi)\,\Phi_o(r,t). \tag{20}$$

At an observation point in the far-field and with the constant vorticity assumption [19], the directional velocity and pressure components can be expressed as:

$$\mathbf{v}_d(r,\theta,\phi,t) = \Gamma_s(\theta,\phi)\,\mathbf{v}_o(r,t) \tag{21}$$

$$p_d(r,\theta,\phi,t) = \Gamma_s(\theta,\phi)\,p_o(r,t) \tag{22}$$

Then, the radiation pattern as measured in the far-field for the directive source is:

$$J_d(\theta,\phi) = |\Gamma_s(\theta,\phi)|^2\,J_o. \tag{23}$$

Using the concept of secondary sources on the wavefront, following the Huygens' principle and the

Kirchhoff-Helmholtz integral, it may be suggested from Eqs. 21 and 22 that, if the omnidirectional velocity field or pressure field and the source directivity function in the far-field at the time $t = c^{-1}R_f$ are known, the directive response of the source can be obtained for $t \geq c^{-1}R_f$.

Following the discussion on the far-field component it is possible to define two different directivity functions. *Analytic* directivity function refers to the directivity function mathematically defined at the source location. *Empirical* directivity function in contrast, is a source directivity function measured at a distance and is thus considered to be free from the contribution of the near-field components.

The discussion above has two important results which will be discussed further in the following section:

1. If an analytic directivity function is given for a directional source, it is possible to excite the model using the velocity field derived from an omnidirectional velocity potential by directional weighting to simulate the directional wave propagation associated with the source.

2. If an empirical directivity function for directional source measured at a given distance in the far-field exists, it may be used to obtain a directional velocity vector field to simulate wave propagation for distances greater than or equal to the measurement distance.

3.2. Source directivity on 2D DWG mesh

As mentioned above, directivity functions are classified into two groups in this paper as *analytic* and *empirical* directivity functions. It is possible to use analytical directivity functions to weight the initial velocity field directly for designating the directional source to excite the DWG mesh with. The empirical directivity functions are valid only at the distance at which the measurement is made. Therefore, sources with known analytical and empirical directivity functions require two different modelling strategies.

3.2.1. Analytic directivity functions

The analytic directivity function can be used for directionally weighting the source volume velocity distribution at the initial excitation stage of the DWG.

While obtaining the impulse response of a modelled virtual room, DGW meshes are usually excited with a low-pass filtered spatial impulse by setting the junction pressures in such a way that the pressure values are symmetrically distributed around a central excitation point. After setting the initial junction pressure distribution, the iteration is started with the scattering step. If all the incoming wave variables are set to zero, the outgoing wave variables are all equal to the initial junction pressure (see Eqs. 5-8), effectively setting each junction as an individual *omnidirectional* source. This allows for a low-pass filtered omnidirectional impulse to be positioned at the excitation point. If a source directivity other than omnidirectional is required, both the junction pressures and the incident wave variables at each junction have to be initialised. However, this may not be suitable for some practical applications as the outgoing wave variables may also be calculated by multiplying a scattering matrix with input wave variables without calculating the junction pressures at all [14].

Therefore, instead of setting both the junction pressures and the incident wave variables, the outgoing wave variables are initialised and the iteration is started with the propagation step instead of the scattering pass. The following strategy is proposed:

1. A bandlimited excitation pulse is selected as the omnidirectional velocity potential. A suitable candidate is symmetric bivariate Gaussian function weighted with the inverse of the density, ρ^{-1}, expressed in the Cartesian coordinates as:

$$\Phi_o(\mathbf{x},\mu,0) = -\frac{1}{2\rho\pi\sigma^2} e^{-\left[(x-\mu_x)^2+(y-\mu_y)^2\right]/\sigma^2}, \quad (24)$$

   where ($\sigma_x^2 = \sigma_y^2 = \sigma^2$) and ($\sigma_{xy}^2 = \sigma_{yx}^2 = 0$). Note that, in order to designate Φ as the initial velocity potential for a sound source, its sign is set to be negative.

2. The x and y components of the initial omnidirectional velocity, $\mathbf{v}_o(\mathbf{x}) = v_x\,\mathbf{u}_x + v_y\,\mathbf{u}_y$, at a given position $\mathbf{x} = (x,y)$ can then be calculated from Eq. 16 with a change of coordinates from polar to Cartesian as:

$$v_x = \frac{x-\mu_x}{\rho\pi\sigma^4} e^{-\left[(x-\mu_x)^2+(y-\mu_y)^2\right]/\sigma^2}, \quad (25)$$

$$v_y = \frac{y-\mu_y}{\rho\pi\sigma^4} e^{-\left[(x-\mu_x)^2+(y-\mu_y)^2\right]/\sigma^2}, \quad (26)$$

3. As 2D DWG meshes are considered for the purpose of this paper, the directivity function is a function of

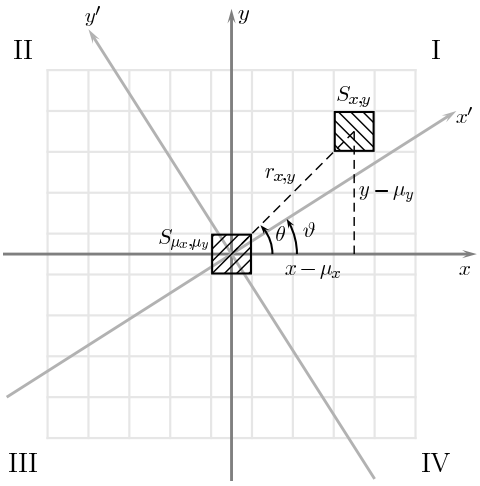

Fig. 2: The conventions used in the derivation of directional velocity vectors. The roman numerals denote the usual quadrant convention

the azimuth angle, θ, only. For a known directivity function $\Gamma_s(\theta)$, at a given position, $\mathbf{x}$, with an arbitrary rotation angle ϑ, the directive velocity vector is obtained as:

$$\mathbf{v}(\mathbf{x},0) = \Gamma_s(\theta-\vartheta)\,[v_{o,x}\ v_{o,y}], \qquad (27)$$

where $\theta = \tan^{-1}(\frac{y-\mu_y}{x-\mu_x})$ (see Fig. 2). It is thus shown that the velocity values at a given scattering junction can be calculated from the selected velocity potential and directivity functions.

4. If the incoming pressure variables for each junction are set to zero, the velocity variables at each port can be defined as:

$$v_N(\mathbf{x},0) = Y\,p^-_{N,x,y}(0), \qquad (28)$$
$$v_S(\mathbf{x},0) = Y\,p^-_{S,x,y}(0), \qquad (29)$$
$$v_E(\mathbf{x},0) = Y\,p^-_{E,x,y}(0), \qquad (30)$$
$$v_W(\mathbf{x},0) = Y\,p^-_{W,x,y}(0), \qquad (31)$$

where Y is the common port admittance. In the original formulation of DWG networks a single velocity variable at a junction is not defined. Therefore we define the x and y components of the *junction velocity* at a given sample time n as:

$$v_x(\mathbf{x},n) = v_E(\mathbf{x},n) - v_W(\mathbf{x},n), \qquad (32)$$
$$v_y(\mathbf{x},n) = v_N(\mathbf{x},n) - v_S(\mathbf{x},n), \qquad (33)$$

consistent with the Cartesian coordinate system. At the initialisation stage these components are:

$$v_x(\mathbf{x},0) = Y\left[p^-_{E,x,y}(0) - p^-_{W,x,y}(0)\right], \qquad (34)$$
$$v_y(\mathbf{x},0) = Y\left[p^-_{N,x,y}(0) - p^-_{S,x,y}(0)\right]. \qquad (35)$$

The following selection is made for convenience: In quadrant I, $p^-_{S,x,y}(0) = p^-_{W,x,y}(0) = 0$, in quadrant II, $p^-_{S,x,y}(0) = p^-_{E,x,y}(0) = 0$, in quadrant III, $p^-_{N,x,y}(0) = p^-_{E,x,y}(0) = 0$, and finally in quadrant IV, $p^-_{N,x,y}(0) = p^-_{W,x,y}(0) = 0$.

Therefore, when the outgoing wave variables are initialised accordingly by using the velocity values obtained from the gradient of the selected velocity potential function, the room impulse response obtained at a given point is that of an excitation by the directive source.

3.2.2. Empirical directivity functions

Far-field directivity functions are usually measured at different angular positions at a fixed distance, $R_f \gg \lambda$, from the sound source in the far-field, where λ is the wavelength. As an example, loudspeaker directivity functions are typically measured at 1 to 2 meters away from the loudspeaker. The directivity of the sound field in the DWG mesh must be equal to the measured directivity function at the *mesh distance* corresponding to the actual measurement distance. The following strategy is proposed:

1. The DWG mesh is first excited with an omnidirectional source. A number of iterations are carried out until the wavefront arrives at the desired measurement position. The wave speed in the 2D rectilinear mesh is defined as:

$$\gamma = c/\sqrt{2}, \qquad (36)$$

where c is the speed of sound (i.e. $c = 344$ m/s). The number of iterations after the excitation moment for the wave to travel a distance of R_f is then:

$$N_i = \left\lfloor \frac{R_f\, f_S}{\gamma} \right\rfloor = \left\lfloor \frac{R_f\, f_S\, \sqrt{2}}{c} \right\rfloor, \qquad (37)$$

where f_S is the temporal sampling rate (i.e. update frequency) of the mesh.

2. The outoing wave variables of the model $p^-_{N,x,y}(N_i-1)$, $p^-_{S,x,y}(N_i-1)$, $p^-_{E,x,y}(N_i-1)$, and $p^-_{W,x,y}(N_i-1)$ with omnidirectional excitation are obtained at the iteration index, N_i-1, and weighted with the empirical directivity function, $\Gamma_s(\theta-\vartheta)$ such that:

$$\hat{p}^-_{N,x,y}(N_i-1) = \Gamma_s(\theta-\vartheta)\, p^-_{N,x,y}(N_i-1), \quad (38)$$

$$\hat{p}^-_{S,x,y}(N_i-1) = \Gamma_s(\theta-\vartheta)\, p^-_{S,x,y}(N_i-1), \quad (39)$$

$$\hat{p}^-_{E,x,y}(N_i-1) = \Gamma_s(\theta-\vartheta)\, p^-_{E,x,y}(N_i-1), \quad (40)$$

$$\hat{p}^-_{W,x,y}(N_i-1) = \Gamma_s(\theta-\vartheta)\, p^-_{W,x,y}(N_i-1), \quad (41)$$

where θ and ϑ are as previously defined. This operation is equivalent to weighting the velocity component of the sound field as in Eq. 27.

3. The obtained directional outgoing wave variables are used to excite the DWG mesh at the next iteration step, N_i. Therefore the empirical directivity function can be observed beginning with the iteration N_i.

It should be noted that the method proposed for the far-field directivity function does not allow the simulation of source directivity before the iteration step, N_i.

4. EXAMPLES

In this section, source directivities for a dipole source and a generic loudspeaker are simulated. For all cases a 900-by-512 rectilinear DWG mesh is used. The boundaries (i.e. walls) of the DWG mesh have a small absorption coefficient, $\alpha \approx 0.12$, and cause phase reversing reflections.

The mesh is excited at the point, $\mu = (260, 256)$ using the velocity vectors obtained from the velocity potential function as described before. The velocity potential function was a bivariate Gaussian with zero covariance terms and the same standard deviation for both variates, $\sigma = 5$ samples. Depending on the type of the source (i.e. analytic or empirical), one of the proposed methods was used for exciting the mesh with a given source directivity function. In order to demonstrate the wave propagation at different iterations, the pressure values on the mesh at the 200, 300, 400, 500, and 600 iteration steps are superimposed in the figures. Figure 3 shows the usual omnidirectional wave propagation pattern at the same iteration steps to allow comparison with the examples that follow.

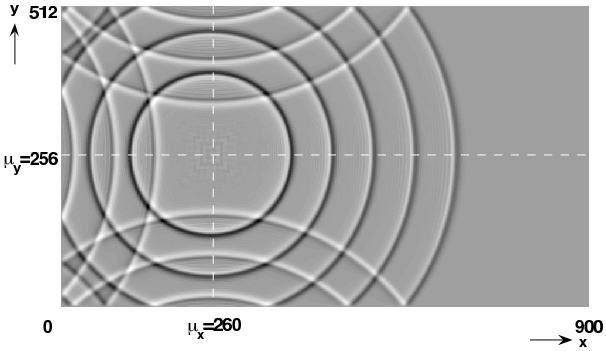

Fig. 3: 2D DWG mesh excited with omnidirectional source.

4.1. Dipole source

A dipole source has a bidirectional (i.e. figure-of-eight) radiation pattern, with the directivity function defined as:

$$\Gamma_s(\theta-\vartheta) = \cos(\theta-\vartheta). \quad (42)$$

Linear combinations of dipole point sources and monopole point sources can be used to express many different source directivities. A loudspeaker on an open-back baffle is a real-life example to a dipole source. Here, dipole directivity function is considered to be analytically defined.

Figure 4(a) shows the dipole directivity function for $\vartheta = 0$. Figure 4(b) shows the wave propagation on the DWG mesh excited using the proposed method for analytic directivity functions. It may be observed that wave propagation is bidirectional in the $\pm x$ direction and that the wave propagation in $-x$ direction has inverted phase (i.e. light color represents negative amplitude and vice versa). The nulls of the directivity function along the $\pm y$ direction may also be observed.

4.2. A generic loudspeaker

Directivity functions of real sources are generally measured in octave and $\frac{1}{3}$-octave bands with a limited angular resolution in the horizontal and vertical planes and interpolated to other angles.

The directivity function used in this example belongs to a generic passive loudspeaker highly directive towards the front direction, measured on the horizontal plane at 1 m distance with 5° intervals in the $\frac{1}{3}$-octave band with $f_C = 2$kHz. A 13^{th}-order polynomial of cosine functions was fit ($r^2 = 0.99$) to the raw directivity data obtained from a CLF (Common Loudspeaker Format) file [20].

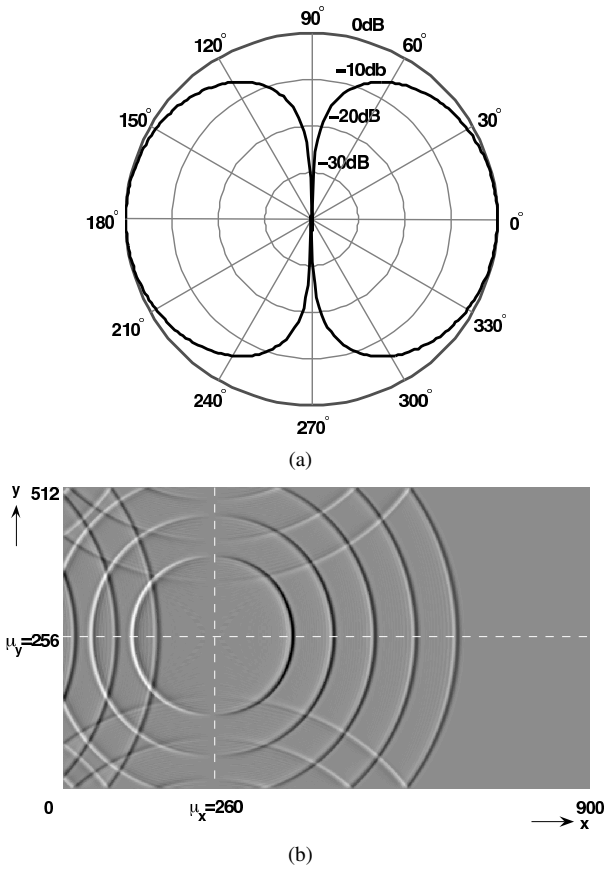

Fig. 4: (a) The directivity function of a dipole source, and (b) 2D DWG mesh excited with a simulated dipole source.

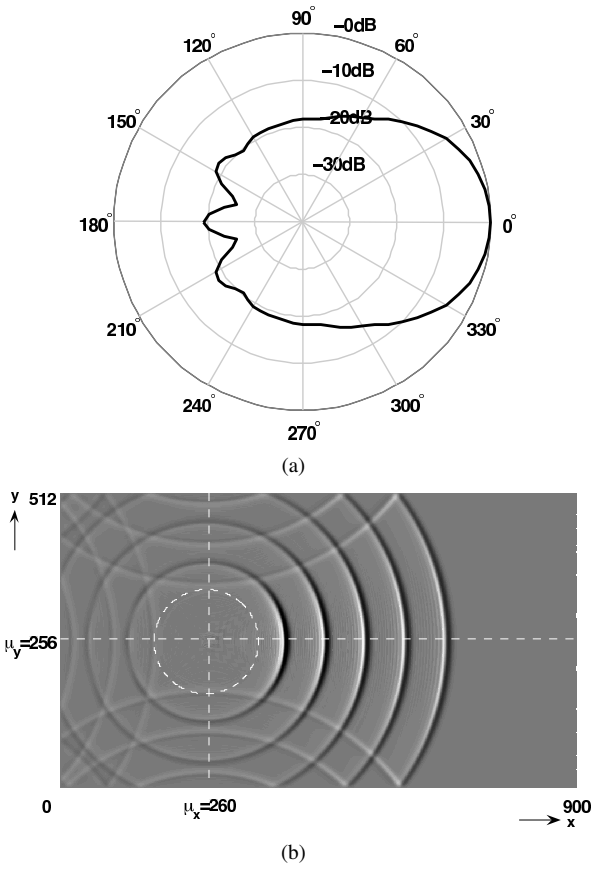

Fig. 5: (a) The directivity function of a generic loudspeaker, and (b) 2D DWG mesh excited with the generic loudspeaker.

Figure 5(a) shows the fitted directivity function. The directivity function of the loudspeaker is empirical. Therefore the model was iterated up to 180 iterations (i.e. $\sim 1\,\mathrm{m}$) before the directional weighting is applied. Figure 5(b) shows the wave propagation on the DWG mesh for the pulse train. The dotted circle shows the distance at which the directivity function measurement was made. It may be observed that, as the directivity function provides around $20-30$ dB attenuation in the back side the wave propagation is strongly directional in the $+x$ direction.

5. DISCUSSION AND CONCLUSIONS

Two simple methods to simulate room impulse responses in DWG meshes, excited by sources with known (i.e. analytic) or measured (i.e. empirical) source directivity functions have been presented in this paper.

The first method pertaining to the simulation of sources with analytic directivity functions is derived from the basic physical notion of velocity potential and are based on the selection of a suitable velocity potential function and obtaining the velocity component of the sound field using the directionally weighted gradient of that function. The resulting velocity vectors are then used to initialise the outgoing wave variables in the DWG mesh which requires starting the DWG iteration not from the scattering, but from the propagation step rather than the scattering pass.

The second method pertaining to the simulation of sources with empirical directivity functions is based on the weighting of the intermediate values of the velocity vectors at a given iteration step corresponding to the

measurement distance on the DWG mesh.

Two examples have been provided of a 2D DWG mesh demonstrating the utility of the proposed method. The first example is the simulation of the directivity of a dipole (i.e. bidirectional) source, and the second example is the simulation of the directivity of a generic loudspeaker. Although the examples were given for a 2D DWG mesh, the method is easily applicable to 3D DWG meshes modelling 3D wave propagation in rooms.

It should be noted that the method proposed for empirical directivity functions is only valid for the impulsive excitation of the DWG mesh and not for an analytical excitation signal which is not concentrated in time. This is due to the fact that for such continuous signals the direct wave front and the reflections will be present in the sound field which is being weighted. This is in contrast with the assumption that the sound field in the travelling direction of the wavefront should be undisturbed.

Direction dependent dispersion is an inherent problem with rectilinearly sampled waveguide meshes. It is especially important as the directional properties of the source is being simulated. One of several existing methods can be applied in order to reduce directional dispersion in rectilinearly sampled DWG meshes to achieve better results [21, 22]. The proposed methods which only depend on the spatial distribution of the wavefront and which are independent of frequency are compatible with such methods.

ACKNOWLEDGMENT

This work was funded by the EPSRC Research Grant GR/S72320/01.

6. REFERENCES

[1] M. Kleiner, B.-I. Dalenbäck, and P. Svensson, "Auralization - an overview," *J. Audio Eng. Soc.*, vol. 41, no. 11, pp. 861–875, 1993.

[2] P. Svensson and U. R. Kristiansen, "Computational modeling and simulation of acoustic spaces," in *Proc. of AES 22nd Int. Conf. on Virtual, Synthetic and Entertainment Audio (AES22)*, Espoo, Finland, 2002, pp. 11–30.

[3] J. L. Flanagan, "Analog measurements of sound radiation from the mouth," *J. Acoust. Soc. Am.*, vol. 32, no. 12, pp. 1613–1620, 1960.

[4] J. Huopaniemi, K. Kettunen, and J. Rahkonen, "Measurement and modelling techniques for directional sound radiation from the mouth," in *Proc. of 1999 IEEE Workshop on Applications of Signal Processing to Audio and Acoustics (WASPAA'99), New Paltz, NY, USA*, 1999, pp. 183–186.

[5] J. Meyer, *Acoustics and the performance of music*. Frankfurt/Main, Germany: Verlag Das Musikinstrument, 1978.

[6] J. B. Allen and D. A. Berkley, "Image method for efficiently simulating small-room acoustics," *J. Acoust. Soc. Am.*, vol. 65, no. 4, pp. 943–950, 1979.

[7] T. Lokki, J. Hiipakka, and L. Savioja, "A framework for evaluating virtual acoustic environments," Presented at the AES 110th Convention, Preprint #5317, Amsterdam, Netherlands, May 2001.

[8] A. Krokstad, S. Strøm, and S. Sørsdal, "Calculating the acoustical room response by the use of a ray tracing technique," *J. Sound Vib.*, vol. 8, no. 1, pp. 118–125, 1968.

[9] J. Mullen, D. Howard, and D. Murphy, "Acoustical simulations of the human vocal tract using 1D and 2D digital waveguide software model," in *Proc. 7th Int. Conf. on Digital Audio Effects (DAFx04)*, Napoli, Italy, 2004, pp. 311–314.

[10] K. Karplus and A. Strong, "Digital synthesis of plucked-string and drum timbres," *Computer Music J.*, vol. 7, no. 2, pp. 43–55, 1983.

[11] J. O. Smith, III, "Physical modeling using digital waveguides," *Computer Music J.*, vol. 16, no. 4, pp. 74–91, 1992.

[12] J. Laird, P. Masri, and C. N. Canagarajah, "Efficient and accurate synthesis of circular membranes using digital waveguides," in *IEE Colloquium on Audio and Music Technology: The Challenge of Creative DSP*, 1998, pp. 12/1–12/6.

[13] L. Savioja, T. Rinne, and T. Takala, "Simulation of room acoustics with a 3-D finite difference mesh," in *Proc. Int. Computer Music Conf. (ICMC'94), Aarhus, Denmark*, 1994, pp. 463–466.

[14] S. Bilbao, *Wave and scattering methods for numerical simulation*. Chichester, UK: John Wiley & Sons, 2004.

[15] D. T. Murphy and D. M. Howard, "Modelling and directionally encoding the acoustics of a room," *Electronics Letters*, vol. 34, no. 9, pp. 864–865, 1998.

[16] A. Kelloniemi, L. Savioja, and V. Välimäki, "Simulation of room acoustics using 2-D digital waveguide meshes," in *2006 IEEE Int. Conf. on Acoustics, Speech and Signal Processing (ICASSP'06)*, vol. 5, 2006, pp. V–313–V–316.

[17] F. Fontana and D. Rocchesso, "Signal-theoretic characterization of waveguide mesh geometries for models of two-dimensional wave propagation in elastic media," *IEEE Trans. on Speech and Audio Processing*, vol. 9, no. 2, pp. 152–161, 2001.

[18] L. Savioja and V. Välimäki, "Interpolated rectangular 3-D digital waveguide mesh algorithms with frequency warping," *IEEE Trans. on Speech and Audio Processing*, vol. 11, no. 6, pp. 783–790, 2003.

[19] A. D. Pierce, *Acoustics: An introduction to its physical principles and applications*. Woodbury, NY, USA: Acoustical Society of America, 1994.

[20] "CLF (Common Loudspeaker Format) Group," `http://www.clfgroup.org`.

[21] L. Savioja and V. Välimäki, "Reduction of the dispersion error in the triangular digital waveguide mesh using frequency warping," *IEEE Signal Processing Letters*, vol. 6, no. 3, pp. 58–60, 1999.

[22] ——, "Multiwarping for enhancing the frequency accuracy of digital waveguide mesh simulations," *IEEE Signal Processing Letters*, vol. 8, no. 5, pp. 134–136, 2001.